



HAL
open science

Electronic Structure and Conductivity of Off-stoichiometric and Si-doped Ge₂Sb₂Te₅ Crystals from Multiple-Scattering Theory

Rajarshi Sinha-Roy, Antonin Louiset, Magali Benoit, Lionel Calmels

► **To cite this version:**

Rajarshi Sinha-Roy, Antonin Louiset, Magali Benoit, Lionel Calmels. Electronic Structure and Conductivity of Off-stoichiometric and Si-doped Ge₂Sb₂Te₅ Crystals from Multiple-Scattering Theory. *Physical Review B: Condensed Matter and Materials Physics (1998-2015)*, 2019, 99 (24), 10.1103/PhysRevB.99.245124 . hal-02160361

HAL Id: hal-02160361

<https://hal.science/hal-02160361>

Submitted on 19 Jun 2019

HAL is a multi-disciplinary open access archive for the deposit and dissemination of scientific research documents, whether they are published or not. The documents may come from teaching and research institutions in France or abroad, or from public or private research centers.

L'archive ouverte pluridisciplinaire **HAL**, est destinée au dépôt et à la diffusion de documents scientifiques de niveau recherche, publiés ou non, émanant des établissements d'enseignement et de recherche français ou étrangers, des laboratoires publics ou privés.

Electronic Structure and Conductivity of Off-stoichiometric and Si-doped $\text{Ge}_2\text{Sb}_2\text{Te}_5$ Crystals from Multiple-Scattering Theory

Rajarshi Sinha-Roy, Antonin Louiset, Magali Benoit, and Lionel Calmels
*CEMES, CNRS, Université de Toulouse, 29 rue Jeanne Marvig, F-31055 Toulouse, France**
(Dated: May 23, 2019)

The transport properties of the phase-change material $\text{Ge}_2\text{Sb}_2\text{Te}_5$ can be tuned by controlling its atomic structure and concentration of charge carriers. Moving away from the “225” stoichiometry or doping with atoms of different chemical species are major methods to reach this aim. The transport properties of these doped samples are challenging to study experimentally, since their crystalline phase generally possesses a complicated microstructure, consisting of grains with different compositions. They are also challenging to investigate by first-principles methods based on the calculation of Kohn-Sham wave functions, as larger supercells are needed to describe the unavoidable chemical disorder among Ge, Sb, dopant atoms, and vacancies. In this work, we perform first-principles calculations of the electronic structure and electrical conductivity of off-stoichiometric or Si-doped cubic $\text{Ge}_2\text{Sb}_2\text{Te}_5$ crystals, using the spin polarized relativistic Korringa-Kohn-Rostoker (KKR) method based on the multiple-scattering theory. The doped crystals have all been described with a rock-salt unit cell, in which the chemical disorder is taken into account through the coherent potential approximation (CPA). The accuracy of the results obtained using this method is verified by comparing, for several crystal compositions, the density of electronic states calculated with this method and with a method that uses Kohn-Sham wave functions and big supercells. We calculated the Bloch spectral function, which shows the dispersion of the electron states and its modification with the deviation from the 225 stoichiometry, silicon doping, and chemical disorder. We describe the composition dependence of the electrical conductivity, which we discuss in terms of the concentration of charge carriers and of the modification of their scattering by the intrinsic chemical disorder in the crystal. These results can be used to model real samples, the microstructure of which consists of grains with different concentrations of Ge, Sb, or Si atoms, each grain being described by a conductivity that depends on its composition.

I. INTRODUCTION

The high contrast between the values of the electrical resistivity of the amorphous and crystalline states of phase change materials (PCMs) can be used to design efficient random access memories (RAMs).¹ In addition to their non-volatility, PCM-based RAMs offer important advantages like scalability, high storage density, and fast reading and writing performances. For recent reviews on PCM and PCM-based RAMs, see references 2 and 3. PCMs have also been used in efficient rewritable optical data storage, owing to the large optical contrast between their amorphous and crystalline phases.⁴

Among the wide family of phase change materials,⁵ germanium-antimony-tellurium (GST) chalcogenide compounds located near the tie-line between GeTe and Sb_2Te_3 in the Ge-Te-Sb phase diagram are particularly interesting and have successfully been used, both in non-volatile resistive memories and in rewriteable optical data storage.^{6,7} They generally present a stable hexagonal phase and a metastable phase with the rock-salt structure. In the latter, one of the two atomic sites of the unit cell is randomly occupied by Ge, Sb, and vacancies, while the other one is occupied by Te atoms.⁸ This description of the metastable phase holds for most of the $[\text{GeTe}]_{(1-x)}[\text{Sb}_2\text{Te}_3]_x$ compounds with $0 < x < 2/3$ and corresponds to a huge fraction of vacancies in the crystal.⁹ Bonding, crystal distortion, chemical species

and vacancy ordering in the hexagonal and cubic phases of most of these compounds have been intensively studied by first-principles methods.^{10,11} Special stacking of GeTe and Sb_2Te_3 , including chemically ordered hexagonal $\text{Ge}_2\text{Sb}_2\text{Te}_5$, have also been reported to behave like topological insulators.^{12,13}

With a fast phase change, a crystallization temperature of 100-150°C, and a melting temperature 600°C,¹⁴ $\text{Ge}_2\text{Sb}_2\text{Te}_5$ shows the best performances along the GeTe - Sb_2Te_3 line, and is one of the most intensively studied GST materials. The precise crystal structure of this 225 compound may depend on the actual crystallization and annealing conditions. The metastable phase shows the rock-salt cubic structure with random distribution of Ge, Sb and vacancies on one of the atomic sites,¹⁵⁻¹⁸ but vacancy ordering can occur in the cubic crystal, leading to different more or less ordered crystalline phases¹⁸⁻²¹ which have also been studied by first-principles methods.²² It has been reported that Ge atoms may also occupy tetrahedral atomic sites instead of octahedral ones in the cubic crystal.²³ However, this issue is still controversial,^{24,25} and the occurring of this defect is not abundant in atomistic DFT simulations of the crystallization process.²⁶⁻²⁸ Above 250°C, $\text{Ge}_2\text{Sb}_2\text{Te}_5$ changes its phase from metastable cubic to stable hexagonal,²⁹ for which several atomic structures have been proposed which differ by the precise location of Ge and Sb atoms in the successive atomic layers:¹⁶ the actual structure of the hexagonal phase may change

from one sample to the other, and different ordering of Ge and Sb atoms can even coexist within the same sample.^{30,31} The differences in the physical properties of the amorphous, cubic and hexagonal crystalline phases of stoichiometric $\text{Ge}_2\text{Sb}_2\text{Te}_5$ have been studied in great details by several teams.³²⁻³⁴ The density of electron states (DOS) of its cubic phase has also been calculated by first-principles methods³⁵⁻³⁷ and recently measured by photoelectron spectroscopy.³⁷⁻³⁹

Several research teams have further explored the possibilities of improving the performances of PCM-based RAMs, using non-stoichiometric and/or doped $\text{Ge}_2\text{Sb}_2\text{Te}_5$. It has been experimentally shown that the crystallization temperature of samples having a high Ge content is higher than that of $\text{Ge}_2\text{Sb}_2\text{Te}_5$ samples.⁴⁰⁻⁴³ In these samples, excess Ge atoms partly segregate during crystallization. The literature does not give detailed experimental results on slightly Ge-rich or Ge-poor $\text{Ge}_2\text{Sb}_2\text{Te}_5$ samples. The consequences of a deviation of the Sb-content from that of perfect $\text{Ge}_2\text{Sb}_2\text{Te}_5$ has been studied by several experimental teams, who observed that the rock-salt structure of $\text{Ge}_2\text{Sb}_{2+y}\text{Te}_5$ samples is preserved for relatively small deviations from the perfect 225 composition, while the excess of Sb atoms tends to concentrate at grain boundaries for higher Sb contents, leading to an increase of the crystallization temperature.^{44,45} Strong deviations from the 225 stoichiometry can even be responsible for a modification of the phase change, that may directly occur from the amorphous to the hexagonal phase.⁴⁶ The consequences of a small excess or deficiency of Ge or Sb atoms on the density of states of the $\text{Ge}_2\text{Sb}_2\text{Te}_5$ crystal have been studied by first-principles methods, using big supercells to mimic the chemical disorder.³⁶ Finally, even in devices based on a perfectly stoichiometric $\text{Ge}_2\text{Sb}_2\text{Te}_5$ layer, electromigration of the different chemical species, both in the amorphous and the crystalline phases, can be responsible for nonuniform deviations from the ideal composition and for a finite gradient of the Ge, Sb and Te concentrations.⁴⁷

Several methods have been considered to dope $\text{Ge}_2\text{Sb}_2\text{Te}_5$ crystals, the most important one consisting in using nitrogen atoms as the dopant chemical species. Such doping enhances the thermal stability of $\text{Ge}_2\text{Sb}_2\text{Te}_5$, increases its crystallization temperature, crystallization time, electrical resistivity and modifies the optical band gap.⁴⁸⁻⁵³ From a structural point of view, it has been shown that part of the nitrogen atoms/molecules occupy specific sites in the $\text{Ge}_2\text{Sb}_2\text{Te}_5$ crystal,⁵³⁻⁵⁶ while all the others precipitate in the $\text{Ge}_2\text{Sb}_2\text{Te}_5$ grains or at grain boundaries where they form germanium nitrides.^{49-51,57,58}

Alternative routes have further been explored for doping $\text{Ge}_2\text{Sb}_2\text{Te}_5$ with chemical species other than nitrogen. Several teams have, in particular, considered

the consequences of substitution or doping with atoms of the same column in the periodic table as those of Ge, Sb or Te: They have shown that doping with Se,^{59,60} Bi,⁶¹⁻⁶⁸ Sn^{61,66,67,69-76} preserves the rock-salt structure at low dopant-atom concentration, while structural changes and phase separation occur otherwise.

Last but not least, the most intensively studied method for doping $\text{Ge}_2\text{Sb}_2\text{Te}_5$ with chemical species of the same columns as those of Ge, Sb or Te in the Mendeleev table, consisted in using Si atoms. Doping (or substitution of Ge) by Si atoms allows an important improvement of the devices, in particular a lowering of the electrical current inducing the phase change, due to an increase of the resistivity of $\text{Ge}_2\text{Sb}_2\text{Te}_5$.⁷⁷⁻⁸³ It has been shown that Si-doped $\text{Ge}_2\text{Sb}_2\text{Te}_5$ can crystallize in the rock-salt structure, at least at low Si content.^{77,83,84} The stability of the doping-sites have been studied by first-principles methods.⁵³ At higher Si-atom concentration, GST samples can also present a phase separation, with Si-rich phases separating $\text{Ge}_2\text{Sb}_2\text{Te}_5$ domains.^{80,84,85}

In this work, we present calculations of the electronic structure and electrical conductivity of GST crystals with the rock-salt structure and a composition slightly different from that of $\text{Ge}_2\text{Sb}_2\text{Te}_5$ (off-stoichiometric crystals), and possibly doped with Si atoms (Si-doped GST crystals). The calculations are done using the first-principles code SPRKKR.^{86,87} This code is based on the density functional theory (DFT), and on the relativistic Korringa Kohn Rostoker (KKR) Green's function formalism, which is based on the multiple scattering theory and uses the coherent potential approximation (CPA) for describing the disorder between different chemical species occupying the same atomic site.⁸⁸ The KKR-CPA method is different from those based on the Kohn-Sham wave functions of a disordered system described in big supercells. The latter are the first-principles methods that have mostly been used, up to now, to calculate the properties of GST crystals. KKR-CPA possesses the big advantage of explicitly taking into account the inherent random disorder involving Ge, Sb and vacancies within a small crystal cell, while larger simulation cells would be required with other DFT-based methods in order to describe the chemical disorder. Moreover, KKR-CPA naturally allows to calculate the effects of disorder on the electrical conductivity of GST crystals, without using empirical parameters, like the relaxation time τ which is often needed (after neglecting its band index and wave vector dependence) in codes based on the Boltzmann equation.⁸⁹ The KKR-CPA method, however, possesses the disadvantage of neglecting the small local distortions of the rock-salt structure, inherent to the random distribution of different chemical species and vacancies.

After an explanation of the technical details of our calculations in Sec. II, we compare in Sec. III the DOS

curves calculated with the code SPRKKR (using small unit cells, and taking into account the random disorder, but not crystal distortions) with those calculated with conventional first-principles methods (using larger supercells describing the chemical disorder as close as possible to random, taking crystal distortions into account). This comparison allows to validate the results calculated with SPRKKR, which are rather satisfactory despite the fact that crystal distortions are neglected. The electronic structure and the dispersion of the electron states are described in Sec. IV for Ge- or Sb-rich or deficient crystals; the conductivity calculated for these off-stoichiometric crystals is described in this section. Results for Si-doped crystals are shown in Sec. V. We discuss our results in section VI and finally conclude in section VII.

II. THEORETICAL BACKGROUND AND CALCULATION DETAILS

In the following, we first describe the general theoretical background adopted for calculating the physical properties, in particular the electronic structure and electrical conductivity, of doped GST alloys. All the calculations are performed using the code SPRKKR. In this code, the fully relativistic Green's function $G(\mathbf{r}, \mathbf{r}', E)$ is calculated using the KKR-CPA method⁸⁶ and the density-functional theory (DFT). This is a method of choice to calculate the Green's function of GST alloys, as the random chemical disorder inherent to these rock-salt crystals can be efficiently described through the CPA.⁸⁸ Unlike other DFT-based methods which use Kohn-Sham wave functions and sufficiently big supercells, KKR-CPA allows a suitable description of the chemical disorder with relatively small crystal unit cells.

The density of electronic states is obtained directly from the calculated Green's function as⁸⁷

$$n(E) = -\frac{1}{\pi} \Im \text{Tr} \int_{\Omega} d^3r G(\mathbf{r}, \mathbf{r}, E), \quad (1)$$

where, Ω is the volume of the crystal unit cell. The Green's function also gives access to the spectral electron-density function which, for a periodic system, corresponds to the Bloch spectral function (BSF) $A_B(E, \mathbf{k})$.^{90,91} It corresponds to the \mathbf{k} -resolved DOS calculated from the lattice Fourier transform of the Green's function as⁸⁷

$$A_B(E, \mathbf{k}) = -\frac{1}{\pi N} \Im \text{Tr} \sum_{n, n'}^N e^{i\mathbf{k} \cdot (\mathbf{R}_n - \mathbf{R}'_n)} \times \int_{\Omega} d^3r G(\mathbf{r} + \mathbf{R}_n, \mathbf{r} + \mathbf{R}'_n, E), \quad (2)$$

where \mathbf{R}_n and \mathbf{R}'_n are Bravais lattice vectors.

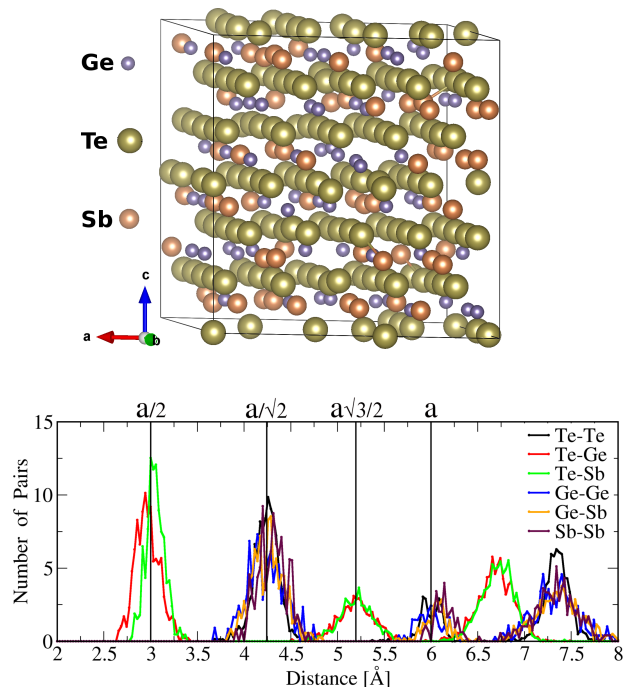


FIG. 1. Top: 300 atomic site supercell relaxed with the code VASP. The \mathbf{c} direction corresponds to the $[111]$ axis of the rock-salt $\text{Ge}_2\text{Sb}_2\text{Te}_5$ crystal, along which layers of Te (yellow) and of Ge (purple) and Sb (orange sphere) atoms are alternatively stacked. Bottom: pair distribution functions calculated for the supercell after relaxation of the atomic coordinates; vertical lines show the first to fourth neighbor distances for the non-distorted crystal.

The zero-temperature dc electrical conductivity tensor can be calculated as the configuration (c) averaged product of the single-electron Green's function and current operator (J) as

$$\sigma_{\mu\nu} = \langle J_{\mu} G J_{\nu} G \rangle_c, \quad (3)$$

where μ, ν are the indices used for the orthogonal space coordinates x, y , and z , and $J_{\mu} = -i\hbar \frac{e}{m} \frac{\partial}{\partial \mu}$. The code SPRKKR employs the Kubo-Greenwood formalism,^{92,93} in order to obtain the symmetric part of the conductivity tensor ($\sigma_{\mu\mu}$, where $\mu \in \{x, y, z\}$) from Eq. (3).^{87,94} A detailed discussion on the implementation of Kubo-Greenwood formalism within the KKR-CPA framework can be found in Ref. 94 and Ref. 95.

We now describe the calculation parameters that have been used to study the GST crystals. We exclusively focused on the face-centered cubic (FCC) rock-salt phase of these compounds. It presents two atomic sites: site A is randomly occupied by Ge, Sb, and vacancies (Vac), and also by Si atoms in the case of Si-doped crystals, while site B is totally occupied by Te atoms. The physical properties of the off-stoichiometric and Si-doped $\text{Ge}_{2+x}\text{Sb}_{2+y}\text{Si}_z\text{Te}_5$ crystals are here mostly

calculated with the code SPRKKR. In this case, the random distribution of the different chemical species and vacancies on site A of the undistorted rock-salt crystal is taken into account through the CPA: scattering potentials are calculated self-consistently in the atomic sphere approximation (ASA), using the generalized gradient approximation (GGA) Perdew-Ernzerhof-Burke^{96,97} (PBE) exchange-correlation energy functional. The CPA potential describing the scattering potential of the atomic site A is calculated within CPA self-consistent loops, from the potentials of Ge, Sb, Si and empty atomic spheres embedded in the CPA crystal, taking their respective concentrations into account, according to the formula $[\text{Ge}_{2+x}\text{Sb}_{2+y}\text{Vac}_{1-x-y-z}\text{Si}_z]_{\text{A}}[\text{Te}_5]_{\text{B}}$. The irreducible wedge of the first Brillouin zone (BZ) has been sampled with 1000 \mathbf{k} -vectors for BZ integrations during the SCF cycles, and with 4000 \mathbf{k} -vectors for the calculations of the DOS and conductivity σ . The Fermi level was accurately determined using Lloyd's formula.⁸⁷ Although this formula helps circumventing problems due to the necessary truncation of the angular momentum expansion of the Green's function for numerical conveniences,⁸⁷ we observed that the convergence of a self-consistent calculation remains difficult to reach when the deviation from the stoichiometry of $\text{Ge}_2\text{Sb}_2\text{Te}_5$ tends to vanish. For this reason, we have chosen to only consider off-stoichiometric and doped GST crystals, for which the Fermi level is clearly either in the conduction band or in the valence band. Green's functions inside the atomic spheres have been expressed in terms of spherical harmonics, up to the maximum angular momentum $l_{max}=2$.

The values of the lattice parameter (and its dependence with Ge, Sb, and Si concentrations) that we used in all the KKR-CPA calculations have formerly been obtained from preliminary calculations based on supercells having 300 atomic sites. Such calculations are indeed more accurate to compute lattice parameters of chemically disordered crystals, as they explicitly allow local atomic structure relaxation due to the actual distribution of Ge, Sb, Si atoms and vacancies on atomic sites A, whereas the KKR-CPA approach is based on a mean-field description of the chemical disorder. The scheme employed for the calculation of the lattice parameter is as follows. The supercell which was built up by stacking 12 FCC (111) atomic layers, consisted of 300 atomic sites, half of which are occupied by Te atoms (on sites B), while others (on sites A) are occupied by Ge, Sb, and dopant Si atoms and vacancies, as shown on the top panel of figure 1. To study GST crystals with concentrations of Ge and Sb atoms deviating from those of $\text{Ge}_2\text{Sb}_2\text{Te}_5$ and doped with Si atoms, we have created different 300 atomic-site supercells, all corresponding to the same composition $\text{Ge}_{2+x}\text{Sb}_{2+y}\text{Si}_z\text{Te}_5$, but with different random distributions of Ge, Sb, and Si atoms on atomic sites A. We only kept the supercell of which the pair distribution function is the closest to that of a

perfect random distribution.

The equilibrium positions of the atoms, and the shape and size of each supercell have been obtained using the *ab initio* simulation package VASP^{98,99}. The Kohn-Sham wave functions in these big supercells were calculated at the Gamma point of the BZ, using a plane-wave basis set truncated at a cutoff energy of 275 eV (≈ 20 Ry), and the GGA PBEsol¹⁰⁰⁻¹⁰² functional for exchange and correlation potentials. The atom positions have further been relaxed, minimizing the interatomic forces on each atom, until the forces became smaller than 10^{-3} eV/Å. The lattice parameter is finally obtained from the volume of the relaxed structure. The pair correlation functions describing one of the relaxed supercells are shown on the bottom panel of figure 1. They show that the rock-salt structure is distorted with nearest neighbor distributions that slightly deviate from the value $a/2$ of the undistorted crystal. The choice of the exchange-correlation functional (PBEsol) is solely based on the fact that it gives a lattice parameter for $\text{Ge}_2\text{Sb}_2\text{Te}_5$ closer to the experimental values than those obtained using PBE or the local density approximation (LDA).

III. VALIDITY OF THE KKR-CPA RESULTS FOR GST CRYSTALS

We have checked that the electronic structure calculated with the KKR-CPA method for a non-distorted rock-salt crystal and with a mean-field description of the chemical disorder on site A does not suffer from these limitations of this method. This has been done by comparing the DOS curves calculated with KKR-CPA with those obtained from Kohn-Sham wave functions calculated for the same compositions, but with big supercells that allow for local distortions of the rock-salt structure. This comparison is shown in figure 2, where we compare the DOS curves calculated with the codes SPRKKR and VASP for the Ge-rich and Ge-deficient $\text{Ge}_{2+x}\text{Sb}_2\text{Te}_5$ crystals with $x = -0.2, -0.1, 0.1, \text{ and } 0.2$. In this figure, the DOS curves calculated with SPRKKR are shown with blue lines, while those calculated with VASP are shown with red lines.

We found a good agreement between the DOS curves calculated with the two methods over a wide range of energy, as shown in the left panel of figure 2. The results shown in this figure also agree with those calculated by Caravati et al.,³⁶ for similar systems. The right panel of figure 2 gives more details on the energy range around the Fermi energy (E_F): the DOS curves calculated with SPRKKR agree nicely with those calculated with VASP in the continuum of states where E_F is located. In particular, the x -dependence of the position of E_F in this continuum is the same for the two methods. This indicates that electron states do not strongly depend on the local distortions of the rock-salt structure. The physical

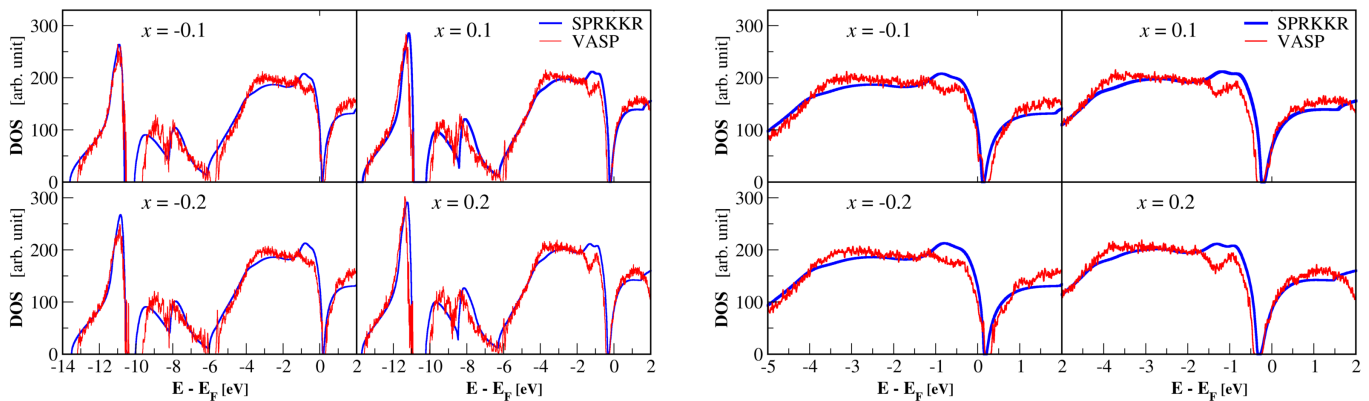


FIG. 2. Left: Density of states calculated with the codes SPRKKR (blue lines), and VASP (red lines) for GST compounds $\text{Ge}_{2+x}\text{Sb}_2\text{Te}_5$ with $x = -0.2, -0.1, 0.1,$ and 0.2 . Right: Same results, but for energies near the fermi level.

information provided by a mean-field description of the disorder, as included in the KKR-CPA method, can further be considered as reliable. However, DOS curves calculated with SPRKKR show small differences with those calculated with VASP, in particular for the continuum of states just above the band gap near E_F for $x < 0$ or just below it for $x > 0$. This can be attributed to the fact that the width of this band gap slightly depends on the calculation method; it may, in particular, slightly depend on the fact that the small distortions of the rock-salt structure are taken into account or not. These small differences do not have strong consequences on the electronic properties of the off-stoichiometric and doped crystals, which all behave like metals for which the concentration of charge carriers depends much more on the deviation from the stoichiometry of $\text{Ge}_2\text{Sb}_2\text{Te}_5$, than on the value of the band gap. However, it is worth mentioning that for a better estimation of the band gap, more elaborated techniques like the use of modified Becke-Johnson exchange potential¹⁰³ or the GW approximation,¹⁰⁴ not available with the code SPRKKR, would be necessary. Within SPRKKR, one could also employ the semi-empirical DFT+U formalism,¹⁰⁵ to have a better description of the band gap. However, this method would require to use empirical U parameters which would increase the complexity of the calculations and necessitate extra care to ensure a reasonable reliability of the results.

IV. EFFECTS OF A MODIFICATION OF THE Ge OR Sb CONCENTRATION

In this section, we describe the physical properties of $\text{Ge}_{2+x}\text{Sb}_2\text{Te}_5$ and $\text{Ge}_2\text{Sb}_{2+y}\text{Te}_5$ GST crystals, in which the concentration of Ge or Sb atoms deviates slightly from that of $\text{Ge}_2\text{Sb}_2\text{Te}_5$.

A. Lattice parameter versus Ge or Sb content

The supercells that have been used to calculate, with the code VASP, the lattice parameter of the GST crystals have been obtained by filling some of the vacancies in the $\text{Ge}_2\text{Sb}_2\text{Te}_5$ 300-atom supercell with Ge or Sb atoms (x or $y > 0$), or by removing Ge or Sb atoms to create additional vacancies (x or $y < 0$). For example, the supercell describing the $\text{Ge}_2\text{Sb}_{2.3}\text{Te}_5$ crystal ($x = 0, y = 0.3$) contains 60 Ge atoms, 69 Sb atoms, 21 vacant sites, and 150 Te atoms; similarly, the supercell corresponding to $\text{Ge}_{1.6}\text{Sb}_2\text{Te}_5$ contains 48 Ge atoms, 60 Sb atoms, 42 vacant sites, and 150 Te atoms ($x = -0.4, y = 0$).

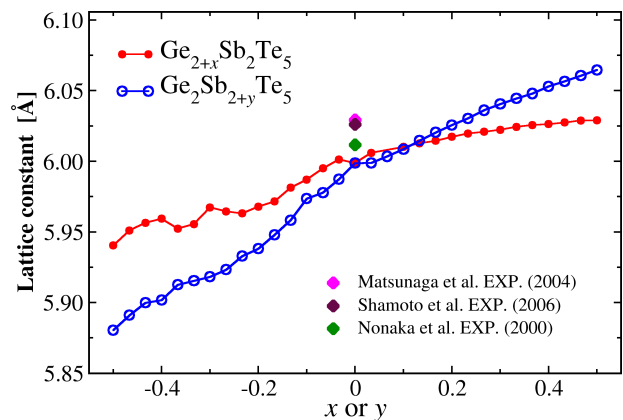


FIG. 3. Lattice parameter calculated with VASP for the GST compounds $\text{Ge}_{2+x}\text{Sb}_2\text{Te}_5$ (in red) and $\text{Ge}_2\text{Sb}_{2+y}\text{Te}_5$ (in blue). Three experimental results are also indicated for $\text{Ge}_2\text{Sb}_2\text{Te}_5$.

The lattice parameters which has been calculated for Ge-rich/deficient GST crystals ($x \neq 0$ and $y = 0$) or Sb-rich/deficient GST crystals (or $x = 0$ and $y \neq 0$) are presented as a function of the composition in figure 3:

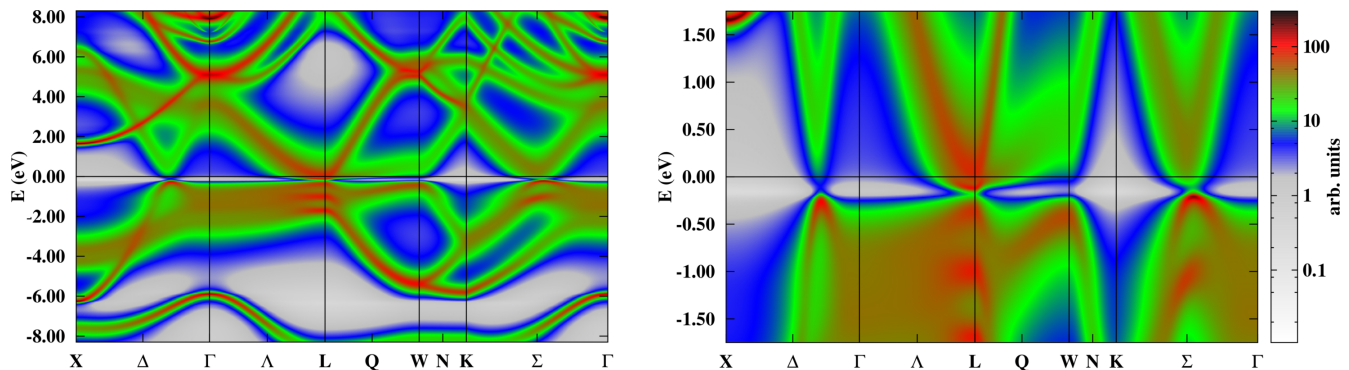


FIG. 4. Bloch Spectral Function calculated for $\text{Ge}_{2.005}\text{Sb}_2\text{Te}_5$ with the code SPRKKR, shown on a wide energy range (left side), and for energies near the Fermi level (right side). $E=0$ corresponds to the Fermi level.

it changes slightly with the composition and this effect is more sensitive to the Sb concentration than to the Ge concentration. This can be traced back to the fact that Sb atoms are larger than Ge atoms: when occupying vacant sites in the supercell, they are responsible for a bigger increase of the volume. In figure 3, we have also shown the lattice parameter of the rock-salt phase of $\text{Ge}_2\text{Sb}_2\text{Te}_5$ measured experimentally by Nonaka et al.,¹⁵ Matsunaga et al.,¹⁶ and Shamoto et al.¹⁰⁶ The calculated lattice parameter is in good agreement with experimental values for this composition.

B. Dispersion and broadening of the electron states versus Ge and Sb content

As already mentioned in section II, the BSF gives a deeper insight to the electronic structure of the GST crystal, since it gives access to the \mathbf{k} -dependence of the electron states and to its modification with disorder. Such information would not have been accessible with a method based on the calculation of Kohn Sham wave functions for supercells, as the dispersion of the electron states, in this case, would have been folded many times on itself and very difficult to analyze.

Broadening of the electron states: Figure 4 shows the BSF calculated for the Ge-rich crystal $\text{Ge}_{2.005}\text{Sb}_2\text{Te}_5$ along the high-symmetry directions of the first Brillouin zone, on a wide energy range on the left panel and for energies near the Fermi level on the right panel. The values of the BSF correspond to the color coding shown on the right hand side of the figure. The BSF becomes vanishingly small in a narrow energy window just below the Fermi level, which corresponds to the band gap found in the literature between the valence and conduction bands of stoichiometric $\text{Ge}_2\text{Sb}_2\text{Te}_5$.^{35,36}

The BSF describes the \mathbf{k} -dispersion of the electron states for a disordered crystal, as the band structure does for a perfectly ordered crystal. Figure 4 shows that

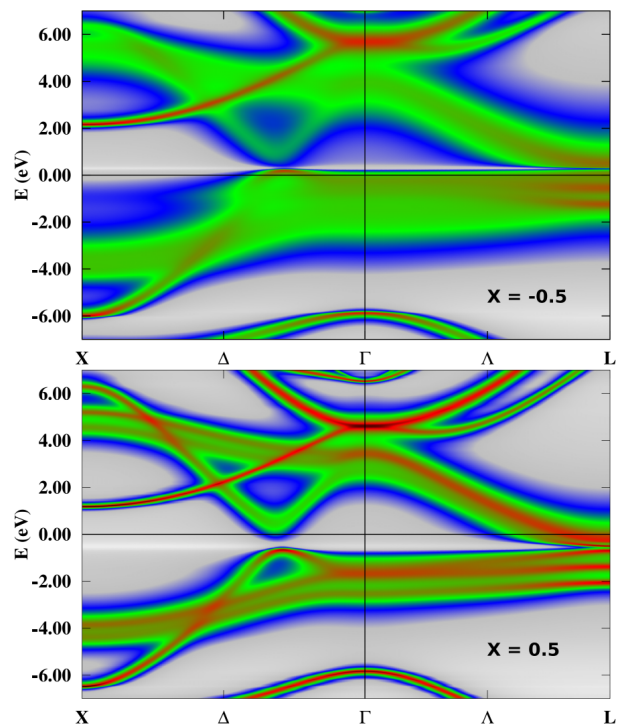


FIG. 5. Bloch Spectral Function calculated with the code SPRKKR for the GST compounds $\text{Ge}_{2+x}\text{Sb}_2\text{Te}_5$ with $x = -0.5$ (upper panel) and $x = 0.5$ (lower panel). $E=0$ corresponds to the Fermi level. The color coding is the same as in fig. 4.

it keeps rather a good recollection of the energy bands that would exist for an ordered crystal, although the chemical disorder between Ge and Sb atoms or vacancies on atomic site A is responsible for a strong broadening of these bands. The maximum value of the BSF (shown in red on figure 4) indicates that different valleys of the conduction band are occupied in the first BZ, in particular near the L-points. From figure 4, we can predict that the main valleys that will be occupied by holes for Ge-poor GST crystals (E_F just below the band

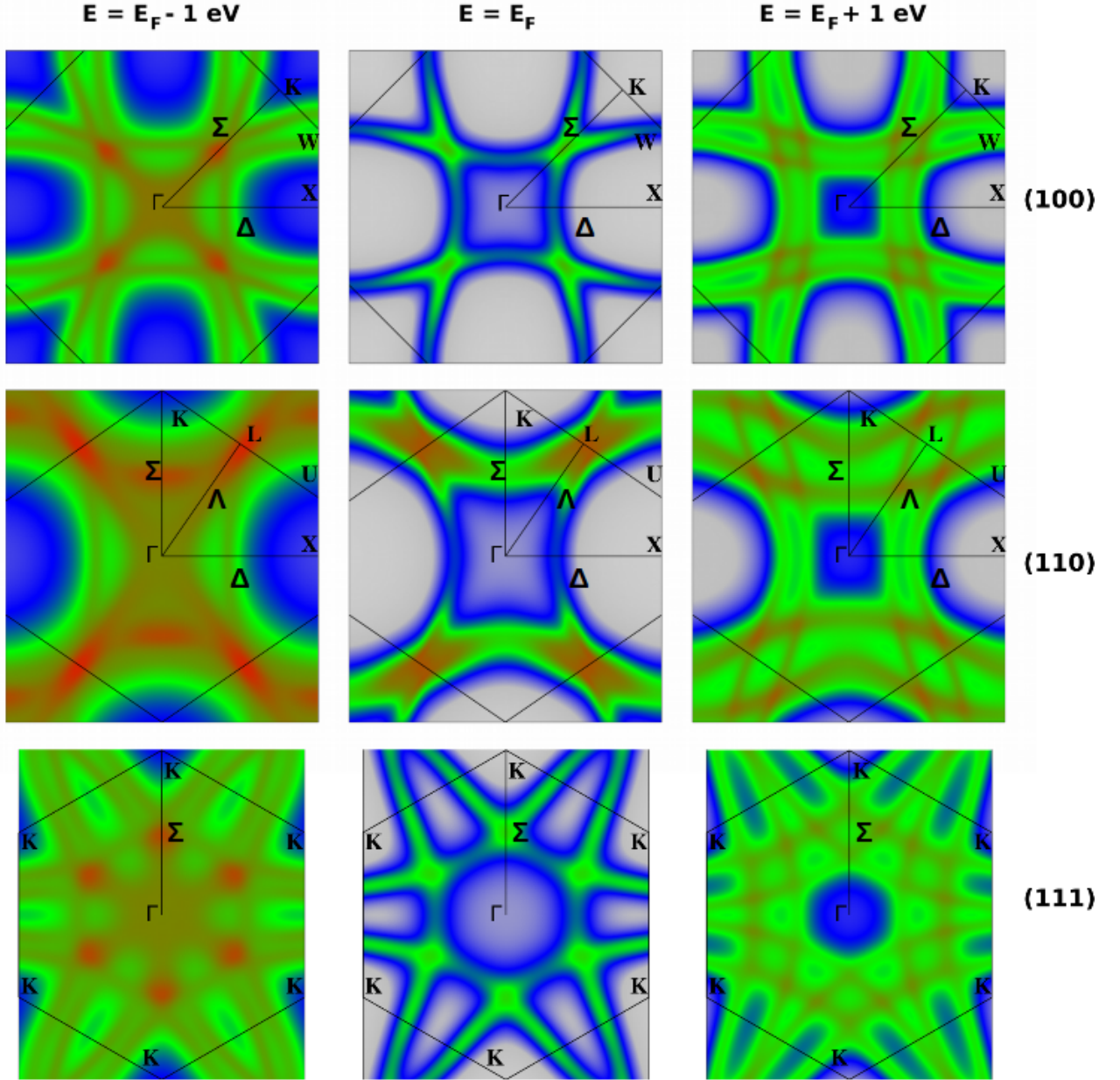


FIG. 6. Map of the Bloch Spectral Function calculated with the code SPRKKR for three different planes of the first BZ of $\text{Ge}_{2.005}\text{Sb}_2\text{Te}_5$: (100) in upper-row panels, (110) in middle-row panels, and (111) in lower-row panels, and for each of them at three different energies: $(E_F - 1 \text{ eV})$ on the left side, E_F in the middle, and $(E_F + 1 \text{ eV})$ on the right side. The color coding is the same as in fig. 4.

gap) will be located at the L-points, at the W-points, between Γ and X-points, and between Γ and K-points.

For a given wave vector, the strong Lorentzian broadening of the electron states shown in figure 4 is inversely proportional to their lifetime τ , and therefore, directly proportional to the imaginary part of the energy.^{94,107,108} This broadening strongly depends on the disorder rate on atomic sites A, as it can be seen

in figure 5, where we compare the BSF of $\text{Ge}_{1.5}\text{Sb}_2\text{Te}_5$ (in this case the Fermi level is in the valence band) and of $\text{Ge}_{2.5}\text{Sb}_2\text{Te}_5$ (for which E_F crosses the conduction band): the reminiscence of the band structure of an ordered crystal is much more clear for the latter. This is due to the fact that vacancies on atomic sites A are a more important cause of electron-state broadening than the statistical disorder between Ge and Sb atoms. We can also notice in this figure that the broadening depends

on the energy E , and on the wave vector \mathbf{k} . Chemical disorder does not actually suppress the band gap near E_F at the L-point of the first BZ: the broadening of electron states on both sides of this band gap gives the impression that the band gap vanishes, in particular at higher vacancy-concentration. However, these states remain clearly split (giving rise to the band gap), and the energy difference between them (i. e. the energy width of the band gap) does not seem to decrease when the chemical disorder increases, and thus, does not lead to the suppression of the band gap. The stoichiometry modifies the broadening of electron states on both sides of the band gap, without changing their energy splitting.

Map of the electron states in the first Brillouin zone:

Figure 6 shows a plot of the BSF $A_B(E, \mathbf{k})$ for \mathbf{k} belonging to three different planes in the first BZ of $\text{Ge}_{2.005}\text{Sb}_2\text{Te}_5$ and for three different energies. The three upper panels show the BSF map in the (100) BZ plane containing two perpendicular Δ directions (Γ -X-W-K plane), the middle panels show similar plots for the (110) BZ plane containing Δ , Σ , and Λ directions (Γ -X-U-L plane), and the lower panels show similar plots for the (111) plane containing six Σ directions (Γ -K). The left side, central, and right side columns respectively correspond to the energies ($E_F - 1$ eV), E_F , and ($E_F + 1$ eV). The color coding is exactly the same as in figure 4. Figure 6 helps to perform deeper inspections of the \mathbf{k} -resolved states as compared to figure 4, which only focuses on the high-symmetry directions of the BZ: it confirms that the main valleys occupied by conduction electrons of this metallic Ge-rich GST compound are mostly located at the L points, and between Γ and K points on the Σ directions. Figure 6 also gives additional information on the anisotropy of these valleys, and on the disorder induced broadening of the electron states, which is proportional to their lifetime $\tau(\mathbf{k}, E)$. The figure shows that the Lorentzian broadening actually depends on wave vector and energy. This is a major constraint for calculating accurately the conductivity of a disordered system using the semi-classical Boltzmann transport equation, where τ is generally considered as identical for all the states.^{89,109}

The results presented in figures 4, 5, and 6 can be very useful for experimentalists who measure the dispersion of electron states in GST crystals with photoemission or inverse photoemission techniques. Angle resolved photoemission spectroscopy (ARPES) has, for instance, been recently used to measure the dispersion of the occupied electron states in samples of cubic metastable $\text{Ge}_2\text{Sb}_2\text{Te}_5$.³⁹ Our results shown in figure 6 for the (111) cut of the first BZ near E_F resemble the ARPES measurements presented by these authors.

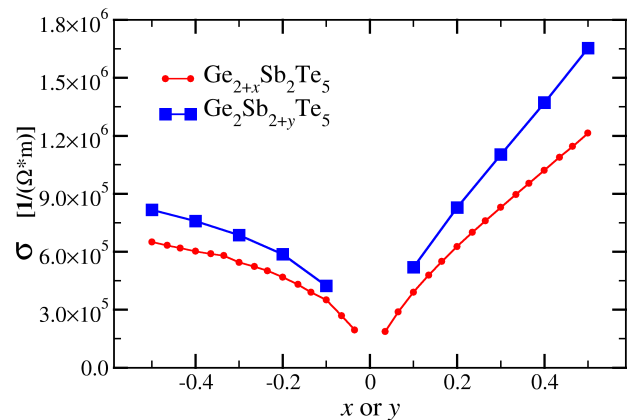


FIG. 7. Electrical conductivity of $\text{Ge}_{2+x}\text{Sb}_2\text{Te}_5$ (in red) and $\text{Ge}_2\text{Sb}_{2+y}\text{Te}_5$ (in blue) GST compounds, as a function of the Ge or Sb concentration.

C. Electrical conductivity versus Ge or Sb content

The dc conductivity σ of the $\text{Ge}_{2+x}\text{Sb}_2\text{Te}_5$ and $\text{Ge}_2\text{Sb}_{2+y}\text{Te}_5$ crystals is represented in figure 7 as a function of the composition for Ge-rich or deficient (red lines) and Sb-rich or deficient (blue lines) compounds. These results have been calculated with the code SPRKKR, using the lattice parameters computed with VASP for the same compositions. These values of the conductivity, which all fall in the range of $10^5 - 10^6$ $[\Omega \cdot m]^{-1}$, have been calculated from ground-state DFT calculations and would correspond to the temperature 0 K. The values of the conductivity that we calculated for off-stoichiometric GST crystals are of the same order of magnitude as those measured for GST crystals in experiments.^{110–112} They are however higher than those measured in experiments. This is not surprising for the two following reasons: firstly, the conductivity has been measured for GST compositions closer to that of $\text{Ge}_2\text{Sb}_2\text{Te}_5$ (i.e. for crystals with a lower densities of charge carriers than in the off-stoichiometric and doped GST crystals that we considered); secondly, we calculated the electrical conductivity at $T=0$ K, while experimental values have been measured at finite temperature (electrons being scattered by phonons, the conductivity of a metal decreases when the temperature increases).

The conductivity has not been explicitly calculated for $\text{Ge}_2\text{Sb}_2\text{Te}_5$ ($x = 0$ and $y = 0$): at the temperature 0 K, this compound being a semiconductor, its conductivity would vanish. As soon as the composition deviates from the stoichiometry of $\text{Ge}_2\text{Sb}_2\text{Te}_5$, the crystal becomes metallic and its conductivity increases. The modification of the conductivity of the GST crystals is due, on the one hand, to changes in the density of the charge carriers, and on the other hand, to modifications of the chemical disorder that scatters the electrons with

an energy near the Fermi level. The density of charge carriers increases with the deviation from the 225 stoichiometry. This increase holds for both x (or y) > 0 (electrons populate the conduction band), and x (or y) < 0 (holes populate the valence band). This tends to increase the conductivity. However, the scattering of the charge carriers by disorder on the atomic site A is higher when there are more vacancies in the crystal, i.e. for Ge- or Sb-poor GST compounds, x (or y) < 0 . This higher disorder-induced scattering of the charge carriers tends to increase the resistivity of the crystal, thus making Ge- or Sb-poor GST compounds less conductive as compared to Ge- or Sb-rich GST compounds, for the same density of charge carriers (i.e., for the same $|x|$ or $|y|$). The conductivity of GST compounds is always higher when Sb atoms have been added to the crystal (or removed) than when the same quantity of Ge atoms have been added (or removed). This is due to the fact that the variations of the number of valence electrons is higher in the former than in the latter case: the electronic structure of an isolated Sb atom is $[\text{Kr}]4d^{10}5s^25p^3$, while that of an isolated Ge atom is $[\text{Ar}]3d^{10}4s^24p^2$.

V. EFFECTS OF Si DOPING

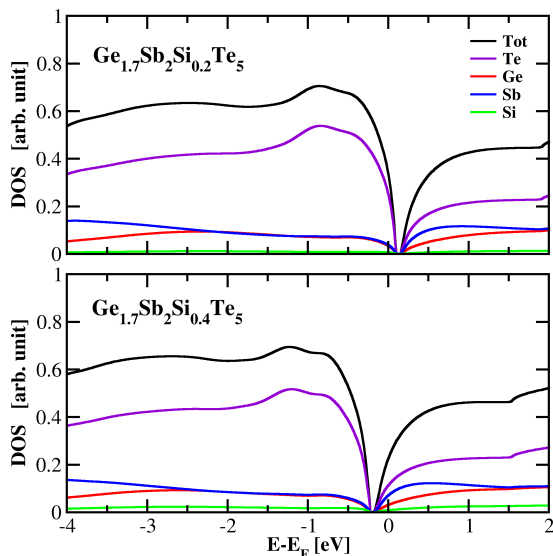


FIG. 8. Total DOS and contribution of each chemical species for $\text{Ge}_{1.7}\text{Sb}_2\text{Si}_{0.2}\text{Te}_5$ (upper panel) and $\text{Ge}_{1.7}\text{Sb}_2\text{Si}_{0.4}\text{Te}_5$ (lower panel).

In this section, we describe the electronic properties of the GST crystals $\text{Ge}_{2+x}\text{Sb}_2\text{Te}_5$, doped with Si atoms. With an electronic structure given by $[\text{Ne}]3s^23p^2$, isolated Si atoms possess the same number of s and p valence electrons as Ge atoms. We first calculated the lattice parameter of Si-doped GST compounds, using the code VASP and the same supercells as those used to study $\text{Ge}_{2+x}\text{Sb}_2\text{Te}_5$, in which some of the vacant sites

have been gradually filled with Si atoms: the calculated lattice parameter (not shown here) increases slightly with the number of Si atoms. It increases, for instance, by 0.3% only between $\text{Ge}_{1.9}\text{Sb}_2\text{Te}_5$ and $\text{Ge}_{1.9}\text{Sb}_2\text{Si}_{0.6}\text{Te}_5$.

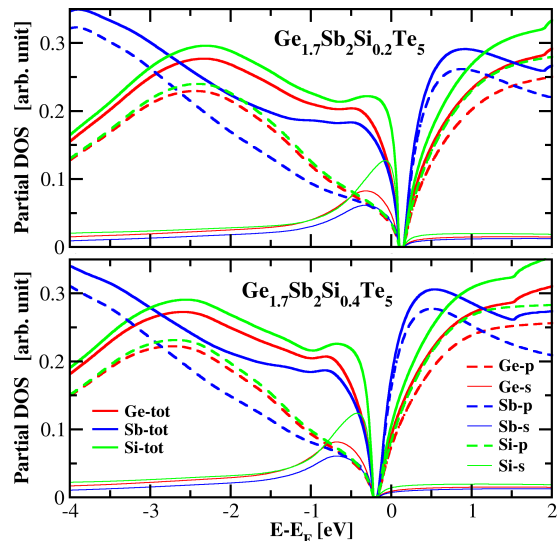


FIG. 9. Contribution of single Ge, Sb, and Si atoms to the DOS of $\text{Ge}_{1.7}\text{Sb}_2\text{Te}_5$ crystals doped with different concentrations of Si atoms. The s and p partial DOS curves are also shown. Upper and lower panels respectively correspond to $\text{Ge}_{1.7}\text{Sb}_2\text{Si}_{0.2}\text{Te}_5$ and $\text{Ge}_{1.7}\text{Sb}_2\text{Si}_{0.4}\text{Te}_5$.

Figure 8 shows the DOS curves calculated for the GST compound $\text{Ge}_{1.7}\text{Sb}_2\text{Si}_z\text{Te}_5$ doped with two different concentrations of Si atoms: $z = 0.2$, for which the Fermi level is below the band gap, and $z = 0.4$, for which it is above it. The doped GST crystals behave like metals for these two compositions. The contribution of the different chemical species is also shown in the figure. The contributions of Ge, Te, and Sb do not strongly change with the concentration of Si atoms. Of course, the contribution of Si is higher for $\text{Ge}_{1.7}\text{Sb}_2\text{Si}_{0.4}\text{Te}_5$ than for $\text{Ge}_{1.7}\text{Sb}_2\text{Si}_{0.2}\text{Te}_5$. Figure 9 shows the total and s- and p-partial DOS per Ge, Sb and Si atom, for the same Si-doped GST crystals as in figure 8. For both crystals, the partial DOS curves are very similar for Si and Ge atoms, with electron bands in exactly the same energy ranges: replacing vacancies by Si instead of Ge atoms does not strongly change the nature of the electron states. We also note in this figure that, whatever the density of Si dopant atoms is, electron states mostly involve p atomic orbitals of Ge, Sb, and Si atoms at energies in the vicinity of the band gap.

The BSF of $\text{Ge}_{2+x}\text{Sb}_2\text{Si}_z\text{Te}_5$ (not shown here) is very similar to that of $\text{Ge}_{2+x+z}\text{Sb}_2\text{Te}_5$, which confirms that replacing Ge by Si atoms does not strongly increase the broadening of the electron states, despite the additional chemical disorder induced by this substitution.

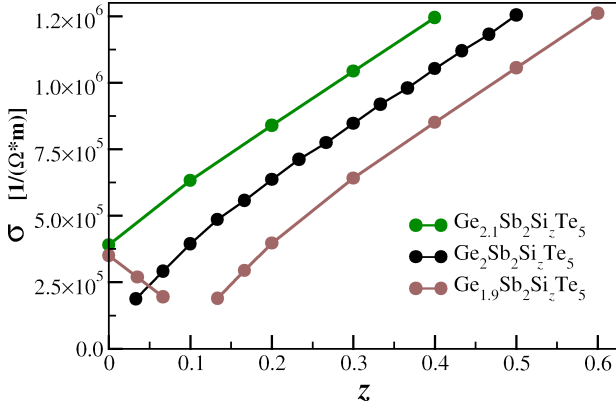


FIG. 10. Electrical conductivity of $\text{Ge}_{2+x}\text{Sb}_2\text{Si}_z\text{Te}_5$ compounds calculated for $x = -0.1$ (in brown), $x = 0.0$ (in black), and $x = 0.1$ (in green) versus concentration of dopant Si atoms.

Figure 10 shows the electrical conductivity of three different $\text{Ge}_{2+x}\text{Sb}_2\text{Si}_z\text{Te}_5$ crystals ($x = -0.1, 0.0,$ and 0.1) as a function of the concentration of dopant Si atoms. The variations of the conductivity as a function of doping depend on the value of x . If $x < 0$ (brown curve), the conductivity first decreases with z up to the critical concentration at which the crystal becomes a semiconductor ($\sigma = 0$ at $T = 0$ K), before increasing again when electrons from additional dopant atoms start populating the conduction band above the band gap. If $x = 0$ (black curve), the undoped crystal is a semiconductor and starts behaving like a metal when dopant atoms are added, which increases the conductivity. If $x > 0$ (green curve), even the undoped crystal is a metal, and doping increases the occupation of the conduction band and the conductivity.

VI. DISCUSSION

In the previous sections, we have described the modifications of the dc conductivity with the concentration of Ge, Sb, or dopant Si atoms in GST crystals near the 225 stoichiometry. We have considered different situations, which all belong to the same general formula $\text{Ge}_{2+x}\text{Sb}_{2+y}\text{Si}_z\text{Te}_5$: the x -, y -, and z -dependences of the conductivity displayed in figures 7 and 10 look very different, and the values shown in these figures strongly depend on the chemical species, the concentration of which is changed with respect to that of $\text{Ge}_2\text{Sb}_2\text{Te}_5$. We now present an overall discussion of these results in terms of the concentration of charge carriers and of the electron scattering induced by chemical disorder in the GST crystal.

Figure 11 shows exactly the same conductivity values as in figures 7 and 10, but plotted as a function of Δn_e , the variation of the number of valence electrons per for-

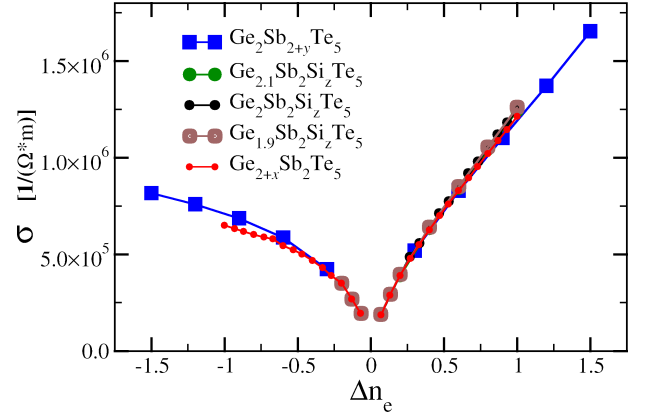


FIG. 11. Conductivity of $\text{Ge}_{2+x}\text{Sb}_{2+y}\text{Si}_z\text{Te}_5$ crystals as a function of Δn_e , the difference in their number of p-valence electrons per formula unit with respect to $\text{Ge}_2\text{Sb}_2\text{Te}_5$.

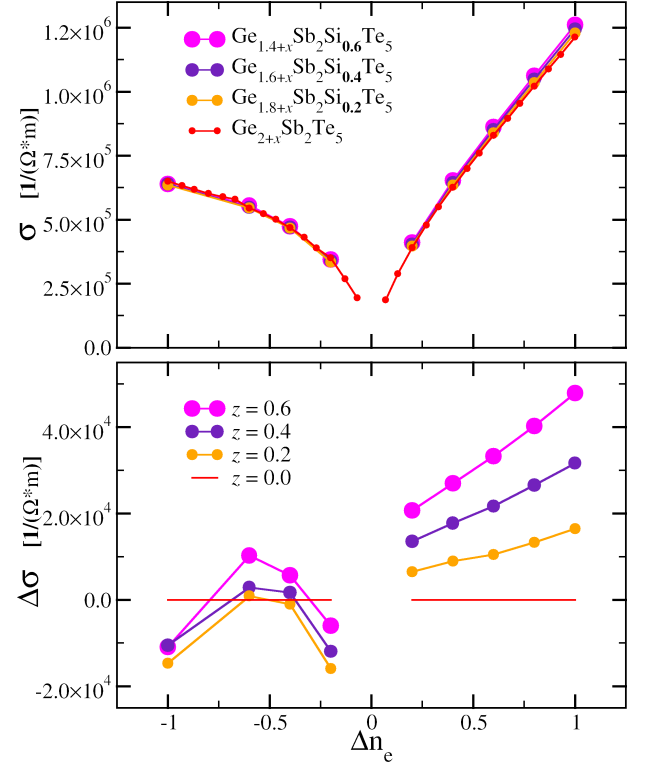


FIG. 12. Top: electrical conductivity of $\text{Ge}_{2+x-z}\text{Sb}_2\text{Si}_z\text{Te}_5$ crystals for $z = 0.0$ (red), 0.2 (orange), 0.4 (violet), and 0.6 (magenta), as a function of Δn_e . Bottom: for the same systems, difference between these conductivities and the conductivity of $\text{Ge}_{2+x}\text{Sb}_2\text{Te}_5$.

mula unit, due to the deviation from the 225 stoichiometry and due to Si-doping, in the $\text{Ge}_2\text{Sb}_2\text{Te}_5$ crystal. In other words, Δn_e is given by

$$\Delta n_e = n_e(\text{Ge}_{2+x}\text{Sb}_{2+y}\text{Si}_z\text{Te}_5) - n_e(\text{Ge}_2\text{Sb}_2\text{Te}_5). \quad (4)$$

We have only considered the number of p-valence elec-

trons of Ge, Sb, and Si atoms to evaluate Δn_e , since the electron states near E_F that become occupied or unoccupied when x , y and z vary, mostly involve the p-orbitals of these atoms, as shown in figure 9. Δn_e is then given by

$$\Delta n_e = 2x + 3y + 2z. \quad (5)$$

Figure 11 shows that all the values of the conductivity that we have calculated for different GST crystals, more or less belong to the same curve when plotted as a function of Δn_e . However, non-negligible differences can be observed in figure 11, between the conductivities of GST crystals possessing the same number of p-valence electrons (same value of Δn_e) but different compositions. This is clearly visible from the comparison of the two curves describing the conductivity of $\text{Ge}_{2+x}\text{Sb}_2\text{Te}_5$ (red) and $\text{Ge}_2\text{Sb}_{2+y}\text{Te}_5$ (blue) crystals versus $\Delta n_e < 0$. These differences are due to the differences of chemical disorder in these crystals. To emphasize this last point, we have calculated the conductivity of three different families of Si-doped GST compounds: $\text{Ge}_{1.4+x}\text{Sb}_2\text{Si}_{0.6}\text{Te}_5$, $\text{Ge}_{1.6+x}\text{Sb}_2\text{Si}_{0.4}\text{Te}_5$, and $\text{Ge}_{1.8+x}\text{Sb}_2\text{Si}_{0.2}\text{Te}_5$, which exactly correspond to the same values of $\Delta n_e = 2x$, and to the same concentrations of vacancies on site A. The values of the conductivity of these three families of Si-doped GST crystals are represented in the upper panel of figure 12 as a function of Δn_e . The values of the conductivity for the undoped $\text{Ge}_{2+x}\text{Sb}_2\text{Te}_5$ crystals are also shown in this figure for reference. The differences

$$\Delta\sigma = \sigma(\text{Ge}_{2+x-z}\text{Sb}_2\text{Si}_z\text{Te}_5) - \sigma(\text{Ge}_{2+x}\text{Sb}_2\text{Te}_5) \quad (6)$$

between the conductivities of the Si-doped and undoped GST crystals are shown in the lower panel of figure 12. These differences are only due to the excess of chemical disorder resulting from the substitution of Ge by Si atoms in the crystals. They are more important for $\Delta n_e > 0$, than for $\Delta n_e < 0$. However, the conductivity differences between crystals with the same concentration of valence electrons and the same number of vacancies on atomic sites A are smaller than those between GST crystals with the same number of valence electrons but different concentrations of vacancies (compare, for instance, the conductivity curves of Ge-poor and Sb-poor crystals for the same values of Δn_e in figure 11)

Although figures 11 and 12 have shown that the conductivity of off-stoichiometric or Si-doped GST crystals depend both on the number of valence electrons and on the chemical disorder rate (in particular, the concentration of vacancies in the crystal), this dependence is not easy to analyze. We can, for instance, compare the values of the conductivity with those of the DOS at the Fermi level, represented in figure 13 as a function of Δn_e for the same crystals as in figures 7 and 12. This comparison shows that σ and the DOS at E_F behave quite similarly with Δn_e . However, σ is not only determined by the DOS at E_F : the nature and rate of the chemical

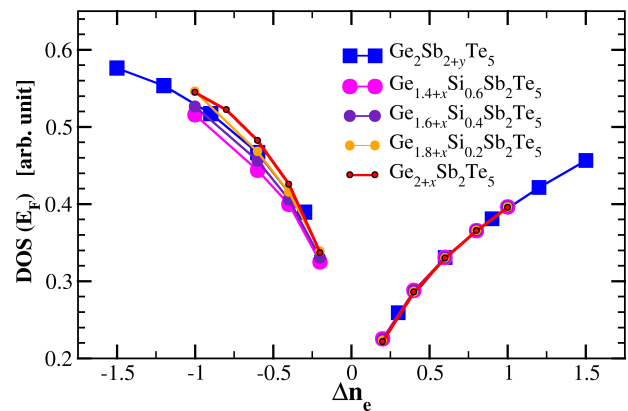


FIG. 13. Density of electron states at E_F as a function of Δn_e for $\text{Ge}_{2+x-z}\text{Sb}_2\text{Si}_z\text{Te}_5$ crystals with $z = 0.0$ (red), 0.2 (orange), 0.4 (violet), and 0.6 (magenta), and for $\text{Ge}_2\text{Sb}_{2+y}\text{Si}_z\text{Te}_5$ crystals (blue).

disorder responsible for electron scattering also play significant role. This has been shown in former theoretical investigations on the conductivity of alloys with random disorder.^{94,113,114}

VII. CONCLUSION

We have presented a numerical study of the electronic structure and conductivity of pure and Si-doped GST crystals, with the rock-salt structure and a stoichiometry close to that of $\text{Ge}_2\text{Sb}_2\text{Te}_5$. The numerical calculations have been performed with the first-principles code SPRKKR, which uses the KKR-CPA method, based on the multiple-scattering theory and on a description of the random disorder among Ge, Sb, Si (dopant) atoms, and vacancies in the crystal through the coherent potential approximation. The accuracy of this method for studying off-stoichiometric and doped GST crystals has been verified, by comparing the DOS curves calculated with this method and with a Kohn-Sham wavefunction based method using supercell in the code VASP. Although KKR-CPA does not take distortions of the rock-salt structure into account, this comparison shows that the DOS curves calculated with the code SPRKKR remarkably agree with their VASP counterparts: this validates the applicability of the KKR-CPA method, with a reasonable accuracy for calculating electronic properties of off-stoichiometric and doped GST crystals. In comparison with Kohn-Sham wave function based methods, the KKR-CPA method is advantageous as it takes less time and less computational resources.

The KKR-CPA method has been applied to Ge- or Sb-rich or deficient GST crystals (with respect to $\text{Ge}_2\text{Sb}_2\text{Te}_5$), which all present a metallic behavior. We have used this method to calculate the Bloch spectral function and the zero-temperature dc electrical conduc-

tivity. The calculated Bloch spectral function has given a clear information on the valleys that will be occupied by charge carriers in these crystals as a function of their composition. The Fermi level is shifted below the band gap for Ge- or Sb-poor GST compounds, and it has been shown that the broadening of the electron states increases in this case with the concentration of vacancies. This broadening is lowered for Ge- or Sb-rich compounds (E_F above the band gap). We have given values for the zero-temperature *dc* electrical conductivity of the off-stoichiometric GST compounds ($\text{Ge}_{2+x}\text{Sb}_2\text{Te}_5$ and $\text{Ge}_2\text{Sb}_{2+y}\text{Te}_5$), and shown that it increases with deviations from the 225 stoichiometry, in particular for Ge- or Sb-rich crystals. We have also described the electronic properties of Si-doped GST compounds and calculated their conductivity. It has been shown that doping with Si atoms has similar effects on the electron states, their broadening, and the conductivity as increasing the concentration of Ge atoms in the crystal. However, Si-doping slightly modifies the conductivity since it increases the chemical disorder.

We have finally shown that the calculated conductivity mostly depends on the overall density of valence p-electrons in the GST crystal, which results both from off-stoichiometry and doping. However, the conductivity

also depends on the intrinsic chemical disorder due to random distribution of Ge, Sb, Si atoms and vacancies. We have shown that, increasing the vacancy concentration has a bigger impact on the conductivity than replacing Ge by Si atoms for the same density of valence electrons. These results, although calculated using a mean-field description of the chemical disorder, show the effects of the chemical composition on the zero-temperature conductivity of GST crystals. We believe that they will be useful in modelling GST samples, with micro-metric grains having compositions close to that of $\text{Ge}_2\text{Sb}_2\text{Te}_5$.

ACKNOWLEDGMENTS

This work was granted access to the HPC resources of CALMIP supercomputing center under the allocation p17025 (2017-2019). This work has been supported through the grant NEXT n° ANR-10-LABX-0037 in the framework of the “Programme des Investissements d’Avenir”. It was also partly funded by Minefi under the Nano 2017 Program. We also acknowledge insightful discussions with Daniel Benoit at STMicroelectronics, Crolles and with Alain Claverie at CEMES, CNRS, Toulouse for having driven our attention to the different technological challenges and aspects from material science perspective.

* rajarshi.sinharoy@cemes.fr, lionel.calmels@cemes.fr

¹ S. R. Ovshinsky, Phys. Rev. Lett. **21**, 1450 (1968).

² G. W. Burr, R. M. Shelby, A. Sebastian, S. Kim, S. Kim, S. Sidler, K. Virwani, M. Ishii, P. Narayanan, A. Fumarola, L. L. Sanches, I. Boybat, M. L. Gallo, K. Moon, J. Woo, H. Hwang, and Y. Leblebici, Advances in Physics: X **2**, 89 (2017), <https://doi.org/10.1080/23746149.2016.1259585>.

³ P. Noé, C. Valle, F. Hippert, F. Fillot, and J.-Y. Raty, Semiconductor Science and Technology **33**, 013002 (2018).

⁴ N. Yamada, E. Ohno, K. Nishiuchi, N. Akahira, and M. Takao, J. Appl. Phys. **69**, 2849 (1991), <https://doi.org/10.1063/1.348620>.

⁵ D. Lencer, M. Salinga, B. Grabowski, T. Hickel, J. Neugebauer, and M. Wuttig, Nature Materials **7**, 972 EP (2008), article.

⁶ M. H. R. Lankhorst, B. W. S. M. M. Ketelaars, and R. A. M. Wolters, Nature Materials **4**, 347 EP (2005), article.

⁷ M. Wuttig and N. Yamada, Nature Materials **6**, 824 EP (2007), review Article.

⁸ N. Yamada, MRS Bulletin **21**, 4850 (1996).

⁹ T. Matsunaga, R. Kojima, N. Yamada, K. Kifune, Y. Kubota, Y. Tabata, and M. Takata, Inorg. Chem. **45**, 2235 (2006), PMID: 16499389, <https://doi.org/10.1021/ic051677w>.

¹⁰ M. Wuttig, D. Lüsebrink, D. Wamwangi, W. Welnic, M. Gilleßen, and R. Dronskowski, Nature Materials **6**, 122 EP (2006), article.

¹¹ J. L. F. Da Silva, A. Walsh, and H. Lee, Phys. Rev. B **78**, 224111 (2008).

¹² B. Sa, J. Zhou, Z. Song, Z. Sun, and R. Ahuja, Phys. Rev. B **84**, 085130 (2011).

¹³ B. Sa, J. Zhou, Z. Sun, J. Tominaga, and R. Ahuja, Phys. Rev. Lett. **109**, 096802 (2012).

¹⁴ E. Morales-Sánchez, E. F. Prokhorov, A. Mendoza-Galván, and J. González-Hernández, J. Appl. Phys. **91**, 697 (2002), <https://doi.org/10.1063/1.1427146>.

¹⁵ T. Nonaka, G. Ohbayashi, Y. Toriumi, Y. Mori, and H. Hashimoto, Thin Solid Films **370**, 258 (2000).

¹⁶ T. Matsunaga, N. Yamada, and Y. Kubota, Acta Crystallographica Section B **60**, 685 (2004).

¹⁷ A. Lotnyk, S. Berntz, X. Sun, U. Ross, M. Ehrhardt, and B. Rauschenbach, Acta Materialia **105**, 1 (2016).

¹⁸ B. Zhang, W. Zhang, Z. Shen, Y. Chen, J. Li, S. Zhang, Z. Zhang, M. Wuttig, R. Mazzarello, E. Ma, and X. Han, Appl. Phys. Lett. **108**, 191902 (2016), <https://doi.org/10.1063/1.4949011>.

¹⁹ V. Bragaglia, F. Arciprete, W. Zhang, A. M. Mio, E. Zallo, K. Perumal, A. Giussani, S. Cecchi, J. E. Boscher, H. Riechert, S. Privitera, E. Rimini, R. Mazzarello, and R. Calarco, Scientific Reports **6**, 23843 EP (2016), article.

²⁰ S. He, L. Zhu, J. Zhou, and Z. Sun, Inorg. Chem. **56**, 11990 (2017), PMID: 28933542, <https://doi.org/10.1021/acs.inorgchem.7b01970>.

²¹ I. Hilmi, A. Lotnyk, J. W. Gerlach, P. Schumacher, and B. Rauschenbach, Materials & Design **115**, 138 (2017).

²² Z. Sun, J. Zhou, and R. Ahuja, Phys. Rev. Lett. **96**, 055507 (2006).

- ²³ X. Q. Liu, X. B. Li, L. Zhang, Y. Q. Cheng, Z. G. Yan, M. Xu, X. D. Han, S. B. Zhang, Z. Zhang, and E. Ma, *Phys. Rev. Lett.* **106**, 025501 (2011).
- ²⁴ J.-Y. Raty, C. Bichara, R. Mazzarello, P. Rausch, P. Zalden, and M. Wuttig, *Phys. Rev. Lett.* **108**, 239601 (2012).
- ²⁵ P. Fons, A. V. Kolobov, J. Tominaga, S. Kohara, M. Takata, T. Matsunaga, N. Yamada, and S. Bokoch, *Phys. Rev. Lett.* **108**, 239603 (2012).
- ²⁶ J. Kalikka, J. Akola, J. Larrucea, and R. O. Jones, *Phys. Rev. B* **86**, 144113 (2012).
- ²⁷ I. Ronneberger, W. Zhang, H. Eshet, and R. Mazzarello, *Advanced Functional Materials* **25**, 6407 (2015).
- ²⁸ J. Kalikka, J. Akola, and R. O. Jones, *Phys. Rev. B* **94**, 134105 (2016).
- ²⁹ W. K. Njoroge, H.-W. Wiltgens, and M. Wuttig, *J. Vac. Sci. Technol. A* **20**, 230 (2002), <https://doi.org/10.1116/1.1430249>.
- ³⁰ I. I. Petrov, R. M. Iamov, and Z. G. Pinsker, *Sov. Phys. Crystallogr.* **13**, 339 (1968).
- ³¹ B. J. Kooi and J. T. M. De Hosson, *J. Appl. Phys.* **92**, 3584 (2002), <https://doi.org/10.1063/1.1502915>.
- ³² K. Shportko, S. Kremers, M. Woda, D. Lencer, J. Robertson, and M. Wuttig, *Nature Materials* **7**, 653 EP (2008), article.
- ³³ T. Kato and K. Tanaka, *Jpn. J. Appl. Phys.* **44**, 7340 (2005).
- ³⁴ B.-S. Lee, J. R. Abelson, S. G. Bishop, D.-H. Kang, B.-k. Cheong, and K.-B. Kim, *J. Appl. Phys.* **97**, 093509 (2005), <https://doi.org/10.1063/1.1884248>.
- ³⁵ J. Akola and R. O. Jones, *Phys. Rev. B* **76**, 235201 (2007).
- ³⁶ S. Caravati, M. Bernasconi, T. D. Khne, M. Krack, and M. Parrinello, *Journal of Physics: Condensed Matter* **21**, 255501 (2009).
- ³⁷ J. Akola and R. O. Jones, *Phys. Status Solidi B* **249**, 1851 (2012).
- ³⁸ C. Pauly, M. Liebmann, A. Giussani, J. Kellner, S. Just, J. Sanchez-Barriga, E. Rienks, O. Rader, R. Calarco, G. Bihlmayer, and M. Morgenstern, *Appl. Phys. Lett.* **103**, 243109 (2013), <https://doi.org/10.1063/1.4847715>.
- ³⁹ J. Kellner, G. Bihlmayer, M. Liebmann, S. Otto, C. Pauly, J. E. Boschker, V. Bragaglia, S. Cecchi, R. N. Wang, V. L. Deringer, P. Küppers, P. Bhaskar, E. Goliias, J. Sánchez-Barriga, R. Dronskowski, T. Fauster, O. Rader, R. Calarco, and M. Morgenstern, *Communications Physics* **1**, 5 (2018).
- ⁴⁰ M. Agati, F. Renaud, D. Benoit, and A. Claverie, *MRS Commun.* **8**, 11451152 (2018).
- ⁴¹ S. Privitera, E. Rimini, C. Bongiorno, R. Zonca, A. Pirovano, and R. Bez, *J. Appl. Phys.* **94**, 4409 (2003), <https://doi.org/10.1063/1.1604458>.
- ⁴² G. Navarro, M. Cou, A. Kioussoglou, P. Noé, F. Fillot, V. Delaye, A. Persico, A. Roule, M. Bernard, C. Sabbione, D. Blachier, V. Sousa, L. Perniola, S. Maitre-jean, A. Cabrini, G. Torelli, P. Zuliani, R. Annunziata, E. Palumbo, M. Borghi, G. Reibold, and B. D. Salvo, *2013 IEEE International Electron Devices Meeting*, **ISSN 2156-017X**, 21.5.1 (2013).
- ⁴³ P. Zuliani, E. Varesi, E. Palumbo, M. Borghi, I. Tortorelli, D. Erbetta, G. D. Libera, N. Pessina, A. Gandolfo, C. Prelini, L. Ravazzi, and R. Annunziata, *IEEE Transactions on Electron Devices* **60**, 4020 (2013).
- ⁴⁴ N. Yamada and T. Matsunaga, *J. Appl. Phys.* **88**, 7020 (2000), <https://doi.org/10.1063/1.1314323>.
- ⁴⁵ K.-J. Choi, S.-M. Yoon, N.-Y. Lee, S.-Y. Lee, Y.-S. Park, B.-G. Yu, and S.-O. Ryu, *Thin Solid Films* **516**, 8810 (2008).
- ⁴⁶ S.-M. Yoon, K.-J. Choi, N.-Y. Lee, S.-Y. Lee, Y.-S. Park, and B.-G. Yu, *Jpn. J. Appl. Phys.* **46**, 7225 (2007).
- ⁴⁷ T.-Y. Yang, I.-M. Park, H.-Y. You, S.-H. Oh, K.-W. Yi, and Y.-C. Joo, *J. Electrochem. Soc.* **156**, H617 (2009), <http://jes.ecsdl.org/content/156/8/H617.full.pdf+html>.
- ⁴⁸ S. Privitera, C. Bongiorno, E. Rimini, and R. Zonca, *Appl. Phys. Lett.* **84**, 4448 (2004), <https://doi.org/10.1063/1.1759063>.
- ⁴⁹ Y. Lai, B. Qiao, J. Feng, Y. Ling, L. Lai, Y. Lin, T. Tang, B. Cai, and B. Chen, *Journal of Electronic Materials* **34**, 176 (2005).
- ⁵⁰ Y. Kim, K. Jeong, M.-H. Cho, U. Hwang, H. S. Jeong, and K. Kim, *Appl. Phys. Lett.* **90**, 171920 (2007), <https://doi.org/10.1063/1.2722203>.
- ⁵¹ M.-C. Jung, Y. M. Lee, H.-D. Kim, M. G. Kim, H. J. Shin, K. H. Kim, S. A. Song, H. S. Jeong, C. H. Ko, and M. Han, *Appl. Phys. Lett.* **91**, 083514 (2007), <https://doi.org/10.1063/1.2773959>.
- ⁵² R. M. Shelby and S. Raoux, *J. Appl. Phys.* **105**, 104902 (2009), <https://doi.org/10.1063/1.3126501>.
- ⁵³ E. Cho, S. Han, D. Kim, H. Horii, and H.-S. Nam, *J. Appl. Phys.* **109**, 043705 (2011), <https://doi.org/10.1063/1.3553851>.
- ⁵⁴ K. Kim, J.-C. Park, J.-G. Chung, S. A. Song, M.-C. Jung, Y. M. Lee, H.-J. Shin, B. Kuh, Y. Ha, and J.-S. Noh, *Appl. Phys. Lett.* **89**, 243520 (2006), <https://doi.org/10.1063/1.2408660>.
- ⁵⁵ S.-J. Kim, J.-H. Choi, S.-C. Lee, B.-k. Cheong, D. S. Jeong, and C. Park, *J. Appl. Phys.* **107**, 103522 (2010), <https://doi.org/10.1063/1.3428362>.
- ⁵⁶ S. Caravati, D. Colleoni, R. Mazzarello, T. D. Khne, M. Krack, M. Bernasconi, and M. Parrinello, *Journal of Physics: Condensed Matter* **23**, 265801 (2011).
- ⁵⁷ T. H. Jeong, M. R. Kim, H. Seo, J. W. Park, and C. Yeon, *Jpn. J. Appl. Phys.* **39**, 2775 (2000).
- ⁵⁸ H. Seo, T.-H. Jeong, J.-W. Park, C. Yeon, S.-J. Kim, and S.-Y. Kim, *Jpn. J. Appl. Phys.* **39**, 745 (2000).
- ⁵⁹ E. M. Vinod, K. Ramesh, and K. S. Sangunni, *Scientific Reports* **5**, 8050 EP (2015), article.
- ⁶⁰ C. Koch, A.-L. Hansen, T. Dankwort, G. Schienke, M. Paulsen, D. Meyer, M. Wimmer, M. Wuttig, L. Kienle, and W. Bensch, *RSC Adv.* **7**, 17164 (2017).
- ⁶¹ T.-J. Park, S.-Y. Choi, and M.-J. Kang, *Thin Solid Films* **515**, 5049 (2007), the Third International Symposium on Dry Process (DPS 2005).
- ⁶² P. Lazarenko, P. Nguyen, H., S. Kozyukhin, and A. Sherchenkov, **13**, 1400 (2011).
- ⁶³ A. Sherchenkov, S. Kozyukhin, A. Babich, and P. Lazarenko, *J. Non-Cryst. Solids* **377**, 26 (2013), iSNOG 2012 Proceedings of the 18th International Symposium on Non-Oxide and New Optical Glasses Rennes, France, July 1-5, 2012.
- ⁶⁴ P. I. Lazarenko, A. A. Sherchenkov, S. S. Kozyukhin, M. Y. Shtern, S. P. Timoshenkov, D. G. Gromov, and E. N. Redichev, *Proc.SPIE* **9440**, 9440 (2014).
- ⁶⁵ S. Kozyukhin, A. Sherchenkov, A. Babich, P. Lazarenko, H. P. Nguyen, and O. Prikhodko, *Can. J. Phys.* **92**, 684 (2014), <https://doi.org/10.1139/cjp-2013-0607>.
- ⁶⁶ K. Wang, C. Steimer, D. Wamwangi, S. Ziegler, M. Wuttig, J. Tomforde, and W. Bensch, *Microsystem Technologies* **13**, 203 (2007).

- ⁶⁷ S. Kozyukhin, M. Veres, H. Nguyen, A. Ingram, and V. Kudoyarova, *Physics Procedia* **44**, 82 (2013), 10th International Conference on Solid State Chemistry, Pardubice, Czech Republic.
- ⁶⁸ J. M. Skelton, A. R. Pallipurath, T.-H. Lee, and S. R. Elliott, *Advanced Functional Materials* **24**, 7291 (2014).
- ⁶⁹ X. Cheng, L. Bo, S. Zhi-Tang, F. Song-Lin, and C. Bomy, *Chinese Physics Letters* **22**, 2929-2932 (2005).
- ⁷⁰ K. Wang, D. Wamwangi, S. Ziegler, C. Steimer, M. J. Kang, S. Y. Choi, and M. Wuttig, *Phys. Status Solidi A* **201**, 3045 (2004).
- ⁷¹ T. J. Park, D. H. Kim, S. M. Yoon, K. J. Choi, N. Y. Lee, B. G. Yu, and S. Y. Choi, *Jpn. J. Appl. Phys.* **45**, L1273 (2006).
- ⁷² M. L. Lee, K. T. Yong, C. L. Gan, L. H. Ting, S. B. M. Daud, and L. P. Shi, *J. Phys. D* **41**, 215402 (2008).
- ⁷³ J. Zhou, Z. Sun, L. Xu, and R. Ahuja, *Solid State Commun.* **148**, 113 (2008).
- ⁷⁴ G. Singh, A. Kaura, M. Mukul, and S. K. Tripathi, *Journal of Materials Science* **48**, 299 (2013).
- ⁷⁵ N. Bai, F. Liu, X. Han, Z. Zhu, F. Liu, X. Lin, and N. Sun, *Applied Surface Science* **316**, 202 (2014).
- ⁷⁶ S. Welzmler, T. Rosenthal, P. Ganter, L. Neudert, F. Fahrnbauer, P. Urban, C. Stiewe, J. de Boor, and O. Oeckler, *Dalton Trans.* **43**, 10529 (2014).
- ⁷⁷ B. Qiao, J. Feng, Y. Lai, Y. Ling, Y. Lin, T. Tang, B. Cai, and B. Chen, *Applied Surface Science* **252**, 8404 (2006).
- ⁷⁸ Q. Bao-Wei, F. Jie, L. Yun-Feng, L. Yun, L. Yin-Yin, T. Ting-Ao, C. Bing-Chu, and C. Bomy, *Chinese Physics Letters* **23**, 172 (2006).
- ⁷⁹ Y. Ling, Y. Lin, B. Qiao, Y. Lai, J. Feng, T. Tang, B. Cai, and B. Chen, *Jpn. J. Appl. Phys.* **45**, L349 (2006).
- ⁸⁰ J. Feng, Y. Zhang, B. Qiao, Y. Lai, Y. Lin, B. Cai, T. Tang, and B. Chen, *Applied Physics A* **87**, 57 (2007).
- ⁸¹ T. Zhang, Z. Song, B. Liu, S. Feng, and B. Chen, *Solid-State Electronics* **51**, 950 (2007).
- ⁸² T. Zhang, Z. Song, F. Rao, G. Feng, B. Liu, S. Feng, and B. Chen, *Jpn. J. Appl. Phys.* **46**, L247 (2007).
- ⁸³ S.-J. Park, I.-S. Kim, S.-K. Kim, S.-M. Yoon, B.-G. Yu, and S.-Y. Choi, *Semiconductor Science and Technology* **23**, 105006 (2008).
- ⁸⁴ S.-M. Jeong, K.-H. Kim, S.-M. Choi, and H.-L. Lee, *Jpn. J. Appl. Phys.* **48**, 045503 (2009).
- ⁸⁵ Y. Jiang, L. Xu, J. Chen, R. Zhang, W. Su, Y. Yu, Z. Ma, and J. Xu, *Phys. Status Solidi A* **210**, 2231 (2013).
- ⁸⁶ H. Ebert and *et al.*, The Munich SPR-KKR package (version 6.3) <http://ebert.cup.uni-muenchen.de/sprkr>.
- ⁸⁷ H. Ebert, D. Kdderitzsch, and J. Minr, *Rep. Prog. Phys.* **74**, 096501 (2011).
- ⁸⁸ P. Soven, *Phys. Rev.* **156**, 809 (1967).
- ⁸⁹ G. K. Madsen and D. J. Singh, *Comput. Phys. Commun.* **175**, 67 (2006).
- ⁹⁰ J. S. Faulkner and G. M. Stocks, *Phys. Rev. B* **21**, 3222 (1980).
- ⁹¹ H. Ebert, A. Vernes, and J. Banhart, *Solid State Commun.* **104**, 243 (1997).
- ⁹² R. Kubo, *J. Phys. Soc. Jpn.* **12**, 570 (1957), <https://doi.org/10.1143/JPSJ.12.570>.
- ⁹³ D. A. Greenwood, *Proc. Phys. Soc.* **71**, 585 (1958).
- ⁹⁴ W. H. Butler, *Phys. Rev. B* **31**, 3260 (1985).
- ⁹⁵ B. Velický, *Phys. Rev.* **184**, 614 (1969).
- ⁹⁶ J. P. Perdew, K. Burke, and M. Ernzerhof, *Phys. Rev. Lett.* **77**, 3865 (1996).
- ⁹⁷ J. P. Perdew, K. Burke, and M. Ernzerhof, *Phys. Rev. Lett.* **78**, 1396 (1997).
- ⁹⁸ G. Kresse and J. Hafner, *Phys. Rev. B* **47**, 558 (1993).
- ⁹⁹ G. Kresse and D. Joubert, *Phys. Rev. B* **59**, 1758 (1999).
- ¹⁰⁰ J. P. Perdew, A. Ruzsinszky, G. I. Csonka, O. A. Vydrov, G. E. Scuseria, L. A. Constantin, X. Zhou, and K. Burke, *Phys. Rev. Lett.* **100**, 136406 (2008).
- ¹⁰¹ J. P. Perdew, A. Ruzsinszky, G. I. Csonka, O. A. Vydrov, G. E. Scuseria, L. A. Constantin, X. Zhou, and K. Burke, *Phys. Rev. Lett.* **102**, 039902 (2009).
- ¹⁰² G. I. Csonka, J. P. Perdew, A. Ruzsinszky, P. H. T. Philipsen, S. Lebègue, J. Paier, O. A. Vydrov, and J. G. Ángyán, *Phys. Rev. B* **79**, 155107 (2009).
- ¹⁰³ F. Tran and P. Blaha, *Phys. Rev. Lett.* **102**, 226401 (2009).
- ¹⁰⁴ L. Hedin, *Phys. Rev.* **139**, A796 (1965).
- ¹⁰⁵ V. I. Anisimov, F. Aryasetiawan, and A. I. Lichtenstein, *Journal of Physics: Condensed Matter* **9**, 767 (1997).
- ¹⁰⁶ S. ichi Shamoto, K. Kodama, S. Iikubo, T. Taguchi, N. Yamada, and T. Proffen, *Jpn. J. Appl. Phys.* **45**, 8789 (2006).
- ¹⁰⁷ B. E. A. Gordon, W. E. Temmerman, and B. L. Gyorffy, *J. Phys. F* **11**, 821 (1981).
- ¹⁰⁸ B. Wiendlocha, *Phys. Rev. B* **88**, 205205 (2013).
- ¹⁰⁹ W. Yu, V. Mauchamp, T. Cabioch, D. Magne, L. Gence, L. Piraux, V. Gauthier-Brunet, and S. Dubois, *Acta Materialia* **80**, 421 (2014).
- ¹¹⁰ R. Fallica, J.-L. Battaglia, S. Cocco, C. Monguzzi, A. Teren, C. Wiemer, E. Varesi, R. Cecchini, A. Gotti, and M. Fanciulli, *Journal of Chemical & Engineering Data* **54**, 1698 (2009), <https://doi.org/10.1021/je800770s>.
- ¹¹¹ W. K. Njoroge, H.-W. Wöltgens, and M. Wuttig, *J. Vac. Sci. Technol. A* **20**, 230 (2002), <https://doi.org/10.1116/1.1430249>.
- ¹¹² I. Friedrich, V. Weidenhof, W. Njoroge, P. Franz, and M. Wuttig, *J. Appl. Phys.* **87**, 4130 (2000), <https://doi.org/10.1063/1.373041>.
- ¹¹³ A.-B. Chen, G. Weisz, and A. Sher, *Phys. Rev. B* **5**, 2897 (1972).
- ¹¹⁴ W. H. Butler and G. M. Stocks, *Phys. Rev. B* **29**, 4217 (1984).